Journal of the Nigerian Association of Mathematical Physics, Volume 9 (November 2005)

FDTD model of acoustic wave interaction with soft targets

Eghuanoye Ikata
Department of Physics, College of Education
P. M. B. 5047, Port Harcourt, Nigeria

Abstract

We have used the finite difference time domain acoustic wave algorithm to study the interaction of a time harmonic acoustic wave with soft acoustic targets. Our interest has been on the character of the acoustic field inside the target and the interaction parameters which influence it. The numerical simulations suggest that for an acoustically denser target the interior field consist of alternate bands of high-(and low-) pressure, though in a narrow cylindrical target the interior is almost completely filled with a high-pressure band. Also, the acoustic field inside the target is influenced by the target aspect ratio, characteristic size and material contrast, such that increasing the aspect ratio and/or characteristic size leads to a significant increase in the interior field magnitude. Provided the aspect ratio is greater than unity and the target is acoustically denser than the exterior medium, the interior acoustic field can attain a magnitude much greater than the amplitude of the incident wave.

PACS: 02.70.Bf – Finite difference methods; 43.35 – Physical effects of sound
pp 545 - 560

1.0 Introduction

The finite difference time domain (FDTD) procedure for the numerical solution of hyperbolic partial differential equation is currently a well-developed and widely used approach for modelling electromagnetic wave interaction with various objects [1]. This method was later adapted to model acoustic wave phenomena [2]. In this work we examine the finite difference time domain acoustic wave algorithm for modelling acoustic wave interaction with various objects with emphasis on how the object geometry and material parameters influence the acoustic field within the object.

An acoustic wave is a disturbance in pressure and density which propagates in a com-pressible medium. When the disturbance is of small magnitude the equations that describe an acoustic wave can be linearized. These are the equation of motion,

$$\rho_0 \frac{\partial \boldsymbol{V}}{\partial t} = -\nabla P\,, \qquad (1.1)$$

and the equation of continuity,

$$\frac{\partial P}{\partial t} = -B\nabla.\boldsymbol{V}\,, \qquad (1.2)$$

where ρ_o and B are, respectively, the equilibrium density and adiabatic bulk modulus of the medium, $\boldsymbol{V}$ is the particle velocity and P is the acoustic pressure. Differentiating (1.2) with respect to time and using (1.1) leads to the wave equation for the acoustic pressure

$$\nabla^2 P = \frac{1}{\upsilon^2}\frac{\partial^2 P}{\partial t^2}, \;\; \upsilon = \sqrt{\frac{B}{\rho_0}}\,, \qquad (1.3)$$

where υ is the wave propagation speed. The product of the wave propagation speed and the equilibrium density gives the characteristic impedance of the medium

$$\eta = \upsilon\rho_0\,. \qquad (1.4)$$

The two coupled first-order partial differential equations (1.1) and (1.2) in a rectangular coordinate system (x, y, z) are equivalent to the set of four coupled partial differential equations:

$$\rho_0 \frac{\partial V_x}{\partial t} = -\frac{\partial P}{\partial x},\ \rho_0 \frac{\partial V_y}{\partial t} = -\frac{\partial P}{\partial y},\ \rho_0 \frac{\partial V_z}{\partial t} = -\frac{\partial P}{\partial z}$$
$$\frac{\partial P}{\partial t} = -B\left(\frac{\partial V_x}{\partial x} + \frac{\partial V_y}{\partial y} + \frac{\partial V_z}{\partial z}\right) \tag{1.5}$$

Equation (1.5) is the basis of a finite difference time domain algorithm for an acoustic wave phenomenon in rectangular coordinates.

A finite difference time domain algorithm approximates the continuous wave field in space and time by sampled data at points in a finite space-time lattice. The derivatives in the differential equation are approximated by finite differences leading to difference equations that replace the differential equations which define a problem. This results in a simulation of the wave by numerical data analogues stored in a computer. An accurate determination of the acoustic field within an arbitrary object is an important problem given the increasing use of ultrasonic signals for diagnosis and therapy in medicine. The numerical experiments show the significance of object aspect ratio and characteristic size on the magnitude of the interior acoustic field, especially when the physical parameters of the object material are grossly different from those of the surrounding medium.

2.0 FDTD acoustic wave algorithm

The common FDTD symbolism introduced by Yee [3] represents a function of space and time as

$$F^n(i,j,k) = F(i\delta x, j\delta y, k\delta z, n\delta t), \tag{2.1}$$

where i, j, k, and n are integers, δx, δy, and δz are space increment along the respective axes, and δt is a time increment. The space and time derivatives are replaced with finite difference approximations which are second-order accurate in the increments using a Taylor series expansion:

$$\frac{\partial F(x_0)}{\partial x} = \frac{F(x_0 + 0.5\delta) - F(x_0 - 0.5\delta)}{\delta} + \vartheta\left(\delta^2\right), \tag{2.2}$$

where x_o is the expansion point and δ is an increment in either space or time.

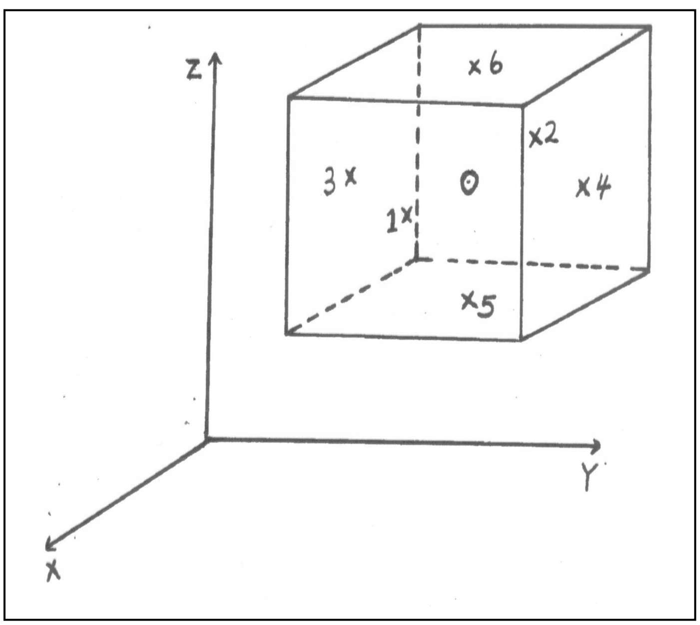

Figure 1: FDTD acoustic wave algorithm unit cell. Body centre point O ≡ *ij,k* for P-field, and face centre points 1 to 6 for *V*-field: 1,2 for V_x, 3,4 for V_y, 5,6 for V_z.

To achieve the accuracy of (2.7) and to realize all the space derivatives, the field components about a cell of the lattice are positioned as shown in Figure 1. To achieve the accuracy of (2.7) for a time derivative the field functions are evaluated at alternate half-time steps. Adopting the half-index scheme and placing the field functions on a lattice as in Figure 1, gives the system of finite difference equations which are an approximation to equation (1.5):

$$
\begin{aligned}
V_x^{n+0.5}(i+0.5,j,k) &= V_x^{n-0.5}(i+0.5,j,k) - \frac{\delta t}{\rho_o \delta x}\left\{P^n(i+1,j,k) - P^n(i,j,k)\right\} \\
V_y^{n+0.5}(i,j+0.5,k) &= V_y^{n-0.5}(i,j+0.5,k) - \frac{\delta t}{\rho_o \delta y}\left\{P^n(i,j+1,k) - P^n(i,j,k)\right\} \\
V_z^{n+0.5}(i,j,k+0.5) &= V_z^{n-0.5}(i,j,k+0.5) - \frac{\delta t}{\rho_o \delta z}\left\{P^n(i,j,k+1) - P^n(i,j,k)\right\} \\
P^{n+1}(i,j,k) &= P^n(i,j,k) - \frac{\mathrm{B}\delta \mathrm{t}}{\delta \mathrm{x}}\left\{\mathrm{V}_{\mathrm{x}}^{\mathrm{n}+0.5}(\mathrm{i}+0.5,\mathrm{j},\mathrm{k}) - \mathrm{V}_{\mathrm{x}}^{\mathrm{n}+0.5}(\mathrm{i}-0.5,\mathrm{j},\mathrm{k})\right\} \\
&\quad - \frac{B\delta t}{\delta y}\left\{V_y^{n+0.5}(i,j+0.5,k) - V_y^{n+0.5}(i,j-0.5,k)\right\} \\
&\quad - \frac{B\delta t}{\delta z}\left\{V_z^{n+0.5}(i,j,k+0.5) - V_x^{n+0.5}(i,j,k-0.5)\right\}
\end{aligned}
\tag{2.3}
$$

The space and time increments are chosen such that the finite difference algorithm is an accurate representation of the differential equations and is stable in time. Usually, the space increment should be a small fraction of the minimum wavelength or object size expected in a model, whichever is smaller. To ensure numerical stability the time increment should satisfy the Courant criterion [4],

$$
\upsilon_{max}\delta t \le \left(\frac{1}{\delta x^2} + \frac{1}{\delta y^2} + \frac{1}{\delta z^2}\right)^{-\frac{1}{2}}, \tag{2.4}
$$

where υ_{max} is the maximum wave speed in the model.

The finite difference equations (2.3) are for updating the field functions at an interior lattice point. In a numerical experiment, the size of the computation space is limited using a lattice truncation scheme [5]. The details on implementing a lattice truncation scheme depend on the kind of problem. Here we implement a second-order Bayliss-Turkel radiation boundary condition [6] along those planes of the lattice boundary normal to the propagation direction and a plane wave (Neumann-type) boundary condition [2] along the remaining planes parallel to the propagation direction. These are discretized using the Mur differencing scheme [7]. For the case where the primary source of the acoustic wave is located outside the problem domain, the wave enters the computation space from outside. This situation is modelled by making a computation boundary plane "radiate" into the computation space, assuming an incident (time harmonic) plane wave.

3.0 Numerical experiments and results

The numerical experiments simulate acoustic wave interaction with an acoustically soft object and model a wave propagating in sea water incident on a piece of quartz immersed in the liquid. The medium exterior to the object is assumed to be infinite, homogeneous and non-dissipative. Our interest is in the (near-) fields in the immediate neighbourhood of an object, especially the interior field within the object. We take the liquid density and bulk modulus to be 998kgm^{-3} and 2.18 x $10^9 Nm^{-2}$, respectively. The medium parameters for quartz are 2650kgm^{-3} and 3.3 x $10^{10} Nm^{-2}$, respectively, for the density and bulk modulus. The angle of incidence in all cases is zero degrees and the wave is incident from the left.

For an incident time harmonic plane wave of wavelength λ, we define an object characteristic size, C.S., equal to a/λ, where *a* is the longitudinal dimension of the object. Here results are presented for simulations in two-dimensions. We have used a square computation space, and the object is positioned within the centre of the computation space such that the lattice truncation is at least ten space increments from the object surface. Time stepping is continued for 3000 time steps or about 72 wave cycles (of the incident wave) basically to test the numerical stability of the algorithm, though it is observed that steady state is achieved much earlier as comparing the results after 800 time steps with that after 3000 time steps revealed. Generally, steady state is achieved relatively earlier for objects with a small characteristic size. We present the result after 1000 time steps. The results show the intensity of the acoustic wave at various computation space grid points after steady state is achieved. To present the field pattern over the entire computation space at a given time the total pressure field at a grid point is translated into an integer which represents the normalized wave intensity.

We distinguish between the 'lit-positive' and 'dark-negative' representations, respectively, to emphasise the broadside and shadow regions. The broadside is that side of an object from which the wave is incident. For the 'lit-positive' representation emphasising the broadside region, a whole number signifies an integer multiple of the incident wave intensity while a 'blank' denotes intensity values less than the incident wave intensity. For the 'dark-negative' representation emphasising the shadow region a whole number denotes a multiple of one-tenth the incident wave intensity while intensity values greater than or equal to the incident wave intensity are denoted by a 'blank'. Thus, on the 'lit-positive' representation a 'blank' is a dark spot while on the 'dark-negative' representation a 'blank' is a bright spot. We use the character '+' to indicate the object surface boundary.

```
11   11   1        11        111  11              1
11   1    1        11        111   1              1
11   1    1        11   1    111   1             11
1    1    1         1   1    11             11   11
1    1    1    1         11    1        11   11   11
     1    1    1         11             11   11   11
          1    1         11             11   111  111
          1    1         11        11   111  1111 111
          1    1    1             11   111  1111 111
          1    1    11            11   111  1111 111
 1                 111       11   111  111  111   11
11    1            11        1111111   111   11   11
11   11            11       11111111   11    11   1
11   11                  11 11111111   11
11   11                 111 1111   11
11   11   11            111  11
11   11   11            111
11  111   11   1        11
1   11   111   1        1
1   11   11    1    1
1   11   11   11   1+++++++++++
1   11   11   11   1+         +
1   11   11   11   1+1        +
1   11   11  121  12+11       +
1   11   11  122  12+11       +
1   11  111  122  12+111      +
1   11   11  122  12+11       +
1   11   11  121  12+11       +
1   11   11   11   1+1        +
1   11   11   11   1+         +
1   11   11   11   1+++++++++++
1   11   11   11    1
1   11   111   1        1
11  111   11   1        11
11   11   11             111    1
11   11   11             111  11
11   11                  111  111  11
11   11                   1   111 111    11
11   11            11         111 111    11    11
11    1            11         11  111  111   11    11
 1                 111       11  111  111  111    11
 1        1    1    11            11  111  1111  11
          1    1    1             11   11   1111 111
          1    1        11             11   1111 111
          1    1        11             11    11  111
     1    1    1        11             11    11   11
1    1    1    1        11    1         1    11   11
1    1    1         1    1   11              1    11
11   1             11     1   11     1             11
11   11            11         111    1              1
11   11            11         111  11
```

Incident from left, direction of propagation

Figure 2(a): Lit-positive representation of normalized intensity for objects of varying characteristic size.
C.S. = 1

3.1 Objects of varying characteristic size

We present a sample of results for numerical experiments which simulate wave interaction with square objects of characteristic size $1.0 \leq C.S. \leq 5.0$; essentially we are concerned with objects whose dimensions are of the same order-of-magnitude as a wavelength. The total field expressed in terms of normalized intensity, over the computation space, are shown in Figures 2 and 3.

```
     1   11        11    1        11  1111 1111 111
    11   11        11            111  1111 1221 122
    1    11    1   11            111  1111 1111 112
         11   11             11  111  1111 1111 111
         11   11             111 111  111  1111 111
 1            11            1111  11   11   11   11
11            11        11  1121  11   11   11   11
11   11                 111 1111  111  11        1
11   11             1   11111111  111
11   11            11   1111111    11
11   11   11       111  111        1
11   11   11      1111  111
1   111   11   1111111   1
1   11    11   111 11
1   11   11   111
1   11   11   1+++++++++++++++++++++
1   11   11   1+                   +
1   11  111  12+1                  +
1   11  121  12+1                  +
1   11  122  12+11         1111    +
2   11  122  12+11        111111   +
21  22   22  12+21       1122211   +
21  221  22   2+21      112222211  +
31  221  221  2+111     112222211  +
31  231  221  1+111     112333221  +
31  231  221  1+111     122333221  +
31  231  221  1+111     112333221  +
31  231  221  1+111     112233221  +
21  221  221  2+211     112222211  +
21  22   22  12+21       11222211  +
2   11  122  12+21       1112111   +
1   11  122  12+11        111111   +
1   11  121  12+11          111    +
1   11  111  12+1                  +
1   11   11  11+1                  +
1   11   11   1+++++++++++++++++++++
1   11   11   111
1   11   111   111 11
1   111   11    111111   1
11   11   11      1111  111
11   11   11       111  111        1
11   11            11   111  11    11
11   11             1   111 1111  11   11
11   11       11        111 1111  11   11   11   11
11            11        11  1111  11   11   11   11
 1            11            1111  11   11  111   11
         11   11             111  11   11  1111 111
         11   11              1  111   11  1111 111
    11   11    1   11            111  111  1111 111
    11   11        11             11  111  1111 112
    11    1        11    1        11  111  1111 111
```

X position, direction of propagation

Figure 2(b): Lit-positive representation of normalized intensity for objects of varying characteristic size. C.S. = 2

Looking at the 'lit-positive' representation, Figure 2(a-e), we observe that the interior pressure field consist mainly of alternate bands of high and low pressure (a kind of fringe pattern). Though for the object with C.S. = 5 the interior seems to be predominantly 'lit-up', being almost completely filled with coalescing high pressure bands. The intensity of the high pressure bands within an object is, usually, greater than that of the incident wave and the maximum attainable magnitude seems to grow monotonically with increasing object characteristic size. Furthermore, the wave penetrates the object with an intensity greater than that of the incident wave.

Examining the 'dark-negative' representation, Figure 3(a - b), we observe that at some interior points the field intensity within a low pressure band can be as low as zero. The relative predominance of such points, with almost zero acoustic wave intensity, seems to be more in objects with a small

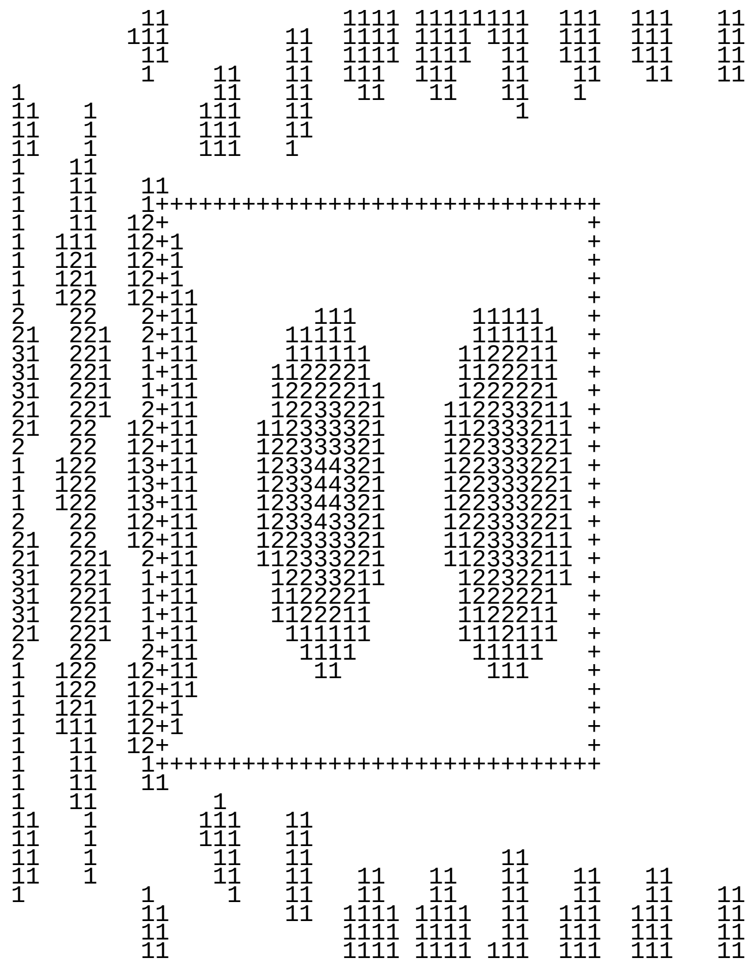

Figure 2(c): Lit-positive representation of normalized intensity for objects of varying characteristic size
C.S. = 3

characteristic size than in those with a large characteristic size. In the shadow region, considering points along a line through the middle of an object, the shadow manifests a variation in intensity (usually called umbra and penumbra in optics). However, relative to the object surface, the first transition from umbra to penumbra is closer to the object surface in those objects with a large characteristic size.

3.2 Problems of varying order-of-magnitude

Here we examined any dependence of the algorithm on the problem order-of-magnitude by looking at wave interaction with objects whose dimensions are measured in millimetre, centimetre, and metre for a fixed characteristic size. Numerical experiments were performed using squares of sides 2 mm, 2 cm and 2 m, for a constant characteristic size, C.S. = 2. The computed results show that the total near-field in a wave interaction with an object is independent of a problem order-of-magnitude provided the object characteristic size is the same. We do not present the intensity patterns for this case.

3.3 Objects of varying aspect ratio

Numerical experiments of wave interaction with rectangular objects were also performed. These experiments reveal the influence of object aspect ratio (A.R.) on the total near-field. We define the aspect ratio as the ratio of length to breadth, where the length is that side of an object transverse to the incident wave direction. For a fixed characteristic size, C.S. = 1, we considered objects with aspect ratios $1 \le A.R. \le 4$.

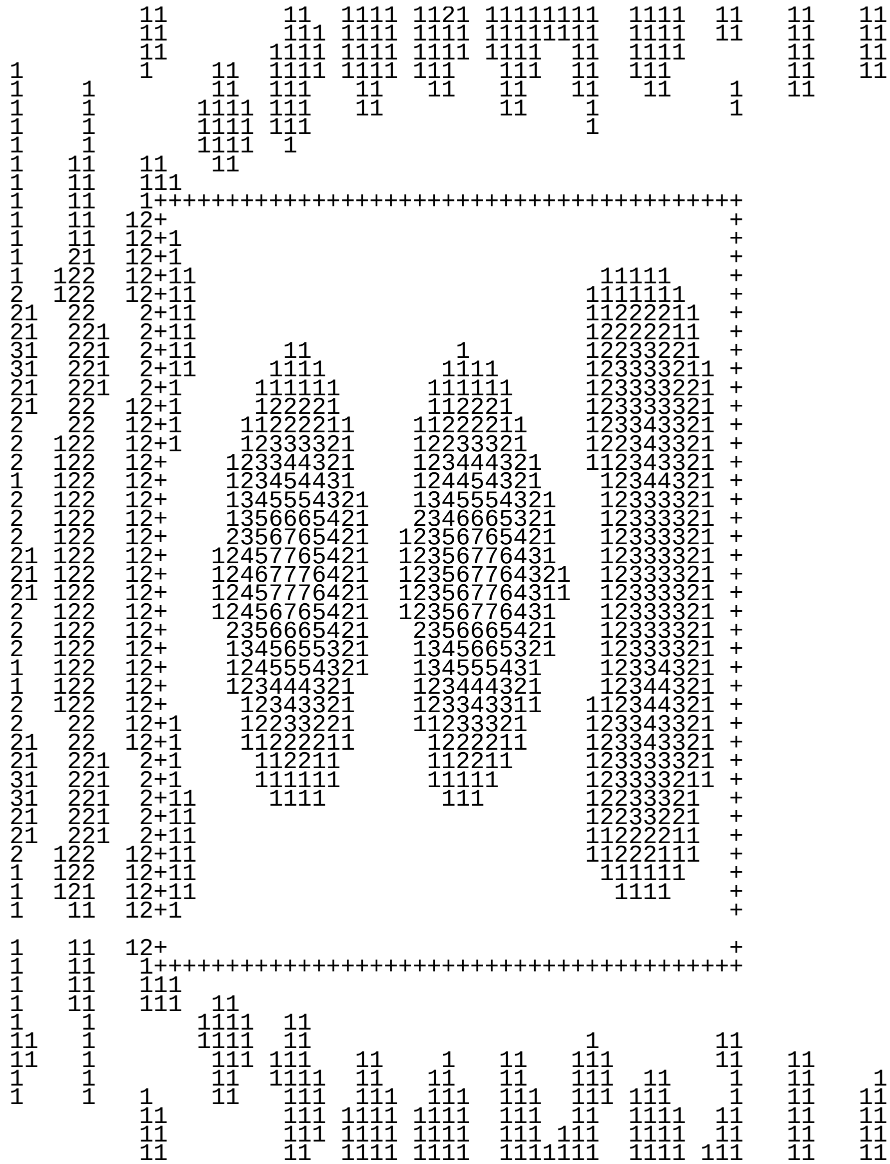

X position, direction of propagation

Figure 2(d): Lit-positive representation of normalized intensity for objects of varying characteristic size. C.S. = 4

Figure 4(a - c) shows the intensity pattern for the 'lit-positive' representation. A striking feature of these results is that the interior acoustic field is a single convex-shaped high pressure band. With increasing aspect ratio the size of this band increases monotonically to fill the interior of the object. Also, the maximum attainable interior field intensity increases monotonically with increasing aspect ratio. Furthermore, it is observed that for $A.R. \ge 3$ there are points in the shadow region where the intensity is as high as that of the incident wave.

Additional experiments were done using objects with A.R. < 1.0. In this case, the interior of the object is almost filled with a low pressure band. The intensity of this band has a maximum near the broadside which tapers to a minimum towards the shadow region. These results are not included here.

```
22  12  11 111 111  11 11112321121112122211221122111211221122
21  21  111111 11   1111222221 122112222211221122111111221122
21  11  11  11  1  11111221221 122112212211221112111111221122
11 111 111  11  1  12111221111112111221111112111111 1111121111
1  11  121  11  1112211121  1111211121  111111 11  111111  11
  111  111  11 1122221 121  111111 111  11  1  11  11  11  11
  11  111   11 1221221 111  11 11   1   1          1
 111  11   11111221111  1   11
 11  11   11111121         111
 11  11  111111111         11
 11  11  2+++++++++++++++++++++++++++++++++++++++
 21  21 13+                                     +
 22  32 13+   1111       1                      +
 22 132 13+1 1122221    111111                  +
 32 133 13+1112344321   12232211          111   +
 33  33  3+1124566431   13344321    111111111111  +
 33  33  3+1135787641   23555321   1111111112221  +
 33  33  2+1246899742  134665421  122221111122211 +
 33  32  2+1247999842  135776421 11233211 1223321 +
 22  22  3+ 258999851  14687642  1234431  1234431 +
 22  22 13+ 258999841  25788631  1355531  1245532 +
 22  22 13+ 258999841  36898631  2467641  1356642 +
 22  22 13+ 158999741 13699852  13688741  14687631+
 22  22 13+ 148999731 14799852  14799852  25899741+
 32  32  3+ 14799963  25899952  36999952  37999841+
 33  32  3+ 14799963  26999952 148999952 159999951+
 43  33 13+ 13799863 136999963125999996212699999962+
 43  43 13+ 136998631137999963237999996213899999972+
 43 143 14+ 136998631148999963248999997324999999982+
 33 143 14+  36998631248999974359999997324999999982+
 33 143 15+  36998631248999974359999997325999999992+
 33 143 15+  36998631248999974359999997325999999982+
 43 143 14+  36998631148999964248999997324999999982+
 43 143 14+ 136998631147999963247999999631399999972+
 43  33 13+ 137998631137999963136999999621379999972+
 33  33  3+ 14799963  3699995212599999962 269999961+
 33  32  3+ 14799963  25899952 137999952 149999951+
 22  32 13+ 14799963  14899852  25899852  36999841+
 22  22 13+ 148999731 14799852  14799741  25798631+
 22  22 13+ 258999741  3689853  13577641  14677531+
 22  22 13+ 258999841  25888631  2456531  1345542 +
 22  22  3+ 258999841  24788641  1345431  1234432 +
 33  22  2+ 248999852  146776421 12343311 1233321 +
 33  33  2+1247999742  135666421  123321111123221 +
 33  33  3+1136898641  124565421  112221111122221  +
 33  33  3+1134677531   23444321   1111111111111  +
 32 133 13+1123455421   12333221    1111  11111   +
 22 132 13+1 12333221   11222111                  +
 22 132 13+  1111111     1111                     +

 21  21 13+                                     +
 11  21  2+++++++++++++++++++++++++++++++++++++++
 11  11  111111111         111
 11  11   11111121         111
 111  11   11111221111  1  111         1
  11  111   11 1221111 111  11111  11   11      1   1   1
  111  111  11  111221 111  111111 111  11 11  11  111 11  11
1  111 111  11  1112211121  1111211121  111111 11  1111111 11
11 111  11  11     12111211111112111211111112111111 1111221122
21  11  111 11  1   1111221111 121112212211221112111111221122
21  12  111111 11   11 1111221 121111122211221122111211221122
22  121 111111 111   1 1111221 111111112211221122111211221122
```

X position, direction of propagation ze

C.S. = 5.

3.4 Experiments with a kidney-shaped object

Based on the experience gained from the earlier experiments we considered experiments which simulate acoustic wave interaction with a 2-D kidney-shaped object. The simulations used a wavelength such that the object characteristic size is equal to unity. The human kidney is essentially bean-shaped, with the average dimensions: length = 11 cm, breadth = 6*cm* and thickness = 3*cm*. In-situ, depending on whether a wave is incident from the front or side of the human host, the kidney has an aspect ratio of about 4 or 2, respectively, if we take a cross-sectional view. Of course, given the shape of the kidney these values do not apply uniformly.

When the object material is quartz, Figure 5(a - b) shows the intensity pattern for the 'lit-positive' representation. Observe that the interior field intensity attains a higher maximum in the object

```
  538  437 73489524  83378525   56  83368523785348
  438 9437 73479525  82279636   559 72268523786359
  438 9437 73479535  7238 746   448 6237852489646
 9339 8337 734796359 6249 846  8337952489635  747
 7349 8338 8348 84588535  9559 62378535  747  858
86359 7349 8348 95578547  9558852378647  858  969
7645896359 8449 95478658  8447742489658  96   97
6655886459 8459 95479768  73467436  76   97    7
6765787569 8459 8558 9779953477548  87   98    7
7975687668 8569 8559  767743589769  97   98    7
9 85589767976699756   6566547  88   97   97   969
  9459 866886788757  95456669       98   869  868
  935  955787778667  7446877        979  868  756 9
  835  955887678767986458  9        979  7569954588
  726  84589766876677547   9    89  867996457743466
  627  736  656886666558   99  96789766886445532344
  429  537  646986566679   879975567644665334432233
  33   339  537 85567779  9657763345533443223321222
 924  923   338 84479888 96434542234321232112211122
 715  814  9239 7359 8766642233311222111211111211111
 616  705  814  725 +++++++++++210111001110111110111
 517  607  606  616 +852100000+10001000011001110111
 517  508  508  608 + 74200000+00000000010001110122
 518  409  40   60  +  6321100+00000000110001110122
 518  409  40   60  +  9532110+00000000110011110133
 418  40   30   60  +   642210+00000000110011211133
 508  409  30   60  +  9642110+00000000110011210133
 508  409  40   60  +  7432110+00000000110011110122
 507  508  508  608 + 85210000+00001000111011210122
 517  607  606  617 +952100000+00011000111011210112
 616  705  814  726 +++++++++++10012100121112211111
 715  814  923  7359 877764224431123211222112211122
 924  923   338 84478878 964456522343212322222321122
  33   339  437 85467679  9657864356533443223321233
  439  527  546986566569   779 85577644564334432244
  528  636  646886666558   88  97799756775445532355
  726  84599756876687546   99   89  867996457743466
  835  945897678767996458 989   9   979  7568853577
  935  955887788657  84468779   9   979  857  64699
  9459 866886789757  95456668  99   97   869  857
9 85589767986699756   7566547  87   97   97   968
8 75688668 8569 8559  767753589658  87   97    79
6865787569 8459 9558 9779963478547  769  97    7
6655886459 8459 95478768  7447743599759  97    7
7645896359 8449 95478658  8447842489647  869  97
86359 7349 8348 95578547  9558952478636  758  869
 7349 8338 8348 84588535  9559 734796359 646  758
 9339 8337 734796459 6249 846  83489634895359 747
  438 9437973478535  7238 746  9458 7337852489636
  438  436973478525  83379635   559 73378523785359
  538  537973489524  83378635   56  843795236853489
```

Incident from left, direction of propagation

Figure 3(a): Dark-negative representation of normalized intensity for objects of varying characteristic size. C.S. =1

with aspect ratio A.R. = 4, as was the case with the rectangular objects. This confirms the influence of the object geometry on the interior field. However when the parameters of the object are those of kidney tissue with material density 1.04×10^3 Kg m^{-3} and characteristic impedance 1.62×10^6 Kg m^{-2} s^{-1} [8], we have the result shown in Figure 6 for the object with aspect ratio equal to 4. Observe that in this case the interior field intensity is very low in magnitude, compared with the result in Figure 5(a). This highlights the influence of material contrast on the magnitude of the maximum attainable interior field intensity in an acoustic wave interaction with an object, in addition to the significance of object geometry.

4.0 Discussion and conclusion

The model examines acoustic wave interaction with a soft target, with special interest on the acoustic field inside the target. The outcome of this numerical experiment suggest that in an acoustic wave interaction with an object the relevant parameters which influence the magnitude of the acoustic field intensity inside the object are the characteristic size, aspect ratio and material contrast. We note that increasing the characteristic size and/or the aspect ratio leads to a significant increase in the interior field intensity. Also, when the physical parameters (density and bulk modulus or characteristic impedance) of the object are much higher than those of the exterior medium, the field intensity inside

```
645798449  834664369867    9        88   97   869
65579844   72377447  78    9    9   98   97   869
766798559  52488558  88    8    89  98   87   858
986688658 8326  668  98   97   868  979  768  757
 9558975676338  769  979  768  647  867 96579964699
  548 8555545   869  86798646874369 755875457743476
  438 8445557   868  855664346532588533564335532354
  339 8436778   757 9633553234421366312443223421233
 924  734898899854677422442123311233201332112221122
 715  625  8766543454211332112211122100221001110111
 516  528 +++++++++++++++++++++++++++++++0001100011
 418  41  +84100000000001110001110000000+0000100011
 31   41  + 5200000000111100001111111110+0000000011
 31   40  + 8310000112232100012233332210+0000000011
 41   50  + 9520001234543210012456665321+0000000011
 60   70  +  620013467875310013589997531+0000000000
 909  909 +  62002479   74100247     742+0000000000
  08   07 +  620136     95200259      62+0000000000
  07   06 +  620149      730037       73+0000000000
  07   05 +  51026       841038       83+1000000000
  07   06 +  51038        41039       94+1000000000
  07   07 +  51149        5114         4+0001100000
  08  90  +  5115         6114         4+0001100011
 809  80  +  5115         6214         4+0001100111
 70   70  +  5116         7215         4+0001100112
 60   60  +  4016         7215         4+0001100122
 70   60  +  4016         7215         4+0001100111
 809  70  +  4015         6215         4+0001100111
  08  90  +  4115         6114         4+0001100011
  07   08 +  4114         5114         4+0001100000
  07   06 +  51149        51049        4+1001100000
  07   05 +  51037       941038       94+1000000000
  07   06 +  51025       830037       83+1000000000
  08   07 +  620148      620026       63+0000000000
 909  909 +  6201359    85200259     952+0000000000
 60   70  +  62001368  9641001479   9741+0000000011
 40   50  +  520012356765310013578886531+0000000011
 41   40  + 9410001223443210012345544321+0000000011
 31   41  + 6200000011222100012222222110+0001100011
 418  41  +94100000000012100011211000000+0001100011
 516  518 +++++++++++++++++++++++++++++++0001110111
 715  626  8667643455312442123321233101231001210112
 924  73489878 864687523553224422355311343112321122
  339 8436777   757  644564235532477422554224432233
  438 9435656   868  855775347633599634675345642355
  548 95455459  868  9669964688536  855886458853477
  558 85676337  768  978  757  647  967  757  64699
 96689757 84259 657  979  969  867  979  869  757
876688658  62488647  87    7    78  98   87   868
665798549  733775469977    8    89  88   87   869
655798548  844775358866    8    9   87   87   869
```

X position, direction of propagation

Figure 3(b): Dark-negative representation of normalized intensity for objects of varying characteristic size. C.S. =3.

the object can be higher than that of the incident wave. Provided the object aspect ratio is greater than unity and it is acoustically denser than the exterior medium, the interior acoustic field can attain a magnitude much greater than the amplitude of the incident wave at certain points. For narrow cylindrical objects aligned transverse to the direction of the incident wave, the interior of the object is almost completely filled with a high pressure band whose intensity is over five times that of the incident wave.

However, depending on the specific physical situation some of the relevant parameters which influence the magnitude of the interior field may not be amenable to variation. For instance, if we consider the ultrasonic treatment of renal stones, the physical parameters of kidney tissue and those of renal stones are fixed, and as such the material contrast is fixed. Also, typically renal stones have a length of 6 mm and a diameter of 2 mm, so the aspect ratio only depends on its orientation with respect to an incident wave. In such a situation, it is only the characteristic size of the object (that is, wavelength or frequency of the incident wave) which can be varied. However, the insight from the significance of the orientation of the incident wave relative to the object can be exploited. Our simulations suggest that after aligning the source to achieve the maximum aspect ratio (with the direction of the incident wave perpendicular to the length of the stone) the source frequency should be adjusted to obtain a high characteristic size, such as to obtain an interior acoustic field of higher magnitude.

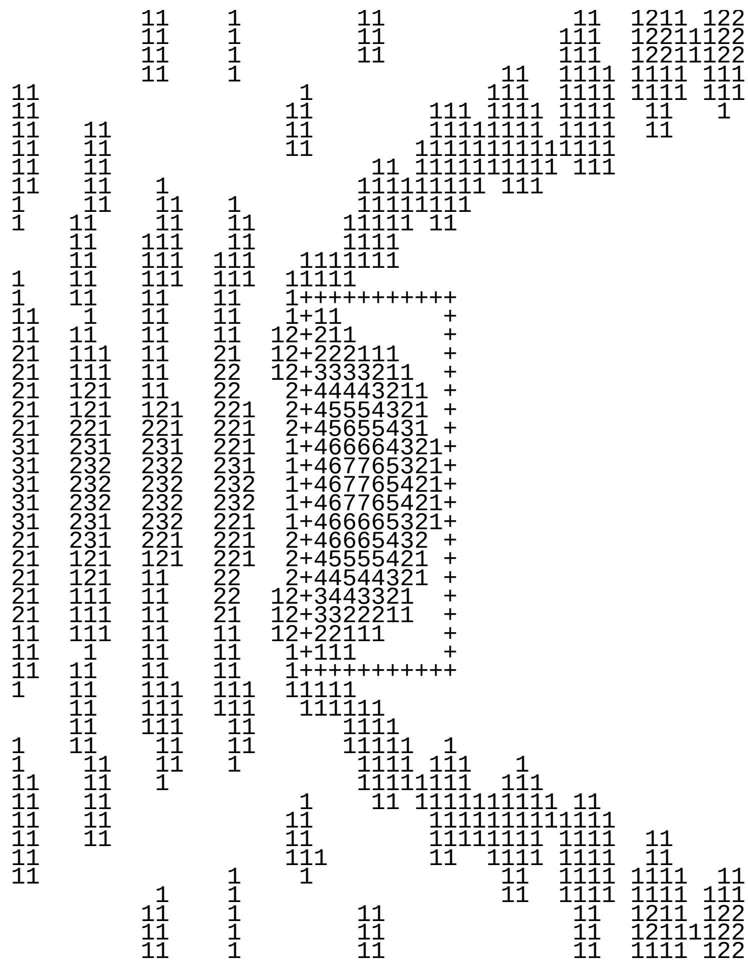

Incident from left, direction of propagation

Figure 4(a): Lit-positive representation of normalized intensity for objects of varying aspect ratio. A.R. = 2,

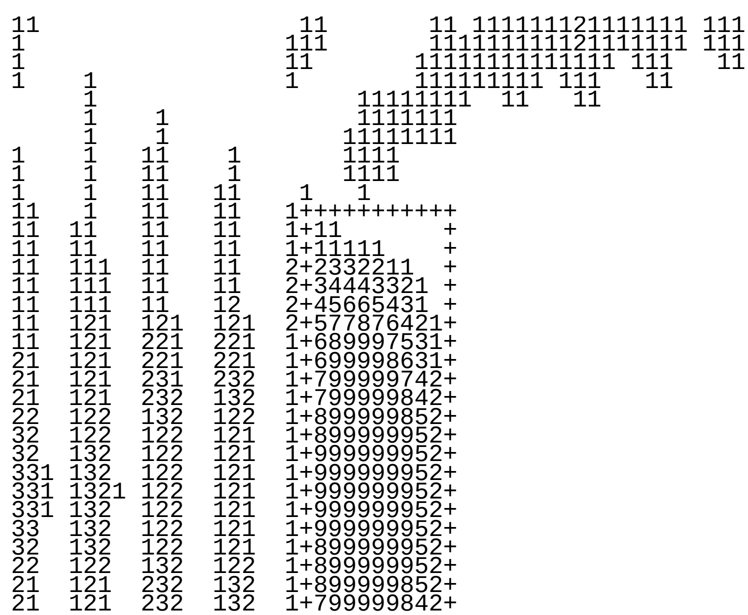

```
21  121  231  231  1+799999741+
11  121  221  221  1+689998631+
11  121  121  121  2+678986531+
11  121  121  121  2+567765321+
11  111  11   11   2+45554321 +
11  111  11   11   2+33333211 +
11  111  11   11   1+222211   +
11  11   11   11   1+111      +
11   1   11   11   1+++++++++++
11   1   11   11    1  111
1    1   11    1       111
1    1   11    1       1111
     1    1             1111 11
     1    1             1111111
     1    1              1111111  11   1
1    1             11       111111111 111    11
1                  11       11111111111111 111    11
11                 111       11111111111111111   11
11                  11          111111121111111 111
```

Incident from left, direction of propagation

Figure 4(b): Lit-positive representation of normalized intensity for objects of varying aspect ratio. A.R. = 3

```
1   11    1             111111111
1   11    1            111111111
1   11    1            11111
1    1   11           1111
1    1   11    1      11
1    1   1    11   1+++++++++++
1    1   1    11   1+11       +
1   11   11   11  12+11111    +
1   11   11   11  12+2222211  +
1   11   11   11   2+34443211 +
1   11   11   11   2+45555421 +
1   11   121  121  1+46777542 +
1   111  121  121  1+579987531+
11  121  121  121  1+689999631+
21  121  121  121  1+699999742+
21  121  121  121   +799999952+
32  122  122  121  1+799999962+
32  122  122  121  1+899999962+
32  122   22   11  1+999999973+
32  1221  22   11  1+999999973+    1
22  122   22  111  1+999999973+   11
22  122  122  121  1+999999983+   11
22  122  121  121  1+999999983+    1
12   11  121  122  1+999999983+        11   11   11
11   11  121  122  1+999999983+        11  111   11
11   11  121  132  1+999999983+        111 111   11
11   11  121  132  1+999999983+        11  111   11
12   11  121  122  1+999999983+        11   11   11
22  122  121  121  1+999999983+    1   11    1
22  122  122  121  1+999999983+   11
22  122   22  121  1+999999983+   11
32  1221  22   11  1+999999973+   11
32  122   22   11  1+999999973+
32  122  122  121  1+899999963+
32  122  122  121  1+899999962+
22  121  121  121   +799999952+
21  121  121  121   +699999852+
11  121  121  121  1+699999741+
11  111  121  121  1+589998631+
1   11   121  121  1+578886421+
1   11   11   12   2+46666532 +
1   11   11   11   2+44554321 +
1   11   11   11  12+3333221  +
1   11   11   11  12+222211   +
1    1   11   11   1+111      +
1    1   11   11   1+++++++++++
1    1   11   11      111
1    1   11    1       111
1   11    1            1111
1   11    1            111111111
1   11    11            111111111
```

Incident from left, direction of propagation

Figure 4(c): Lit-positive representation of normalized intensity for objects of varying aspect ratio. A.R. = 4.

```
  549 845   5479524   659 721574137841389647  858
  549 845   4378525   548 61167513784149 648  858
  548 945  93379636   43785127852378525  758  958
  548 9559 7238 846  832674138952489536  858  869
  438  547 6249 9559952268535  6359 747  958  869
  439  5368625   547741379647  746  969  958  969
 9439 94368636   43563249 858  858   79  968  969
 8348 83369746  83356436  969  97    8  968  969
 8348 7337 8568962367658  979   8    8  979  968
9744896348 955774248 879  979   9    8  97   968
8745886359 95466436   9   979   9    8  97   968
775577646  84456558       979   9   979  87   857
6766776579 7446767        979  989  768  869  757
78767777985458999     89  979  86798657 9757 964699
89766887787547       9779 878  75677546985468753588
9 756888776569       756897679864455445764346533466
  75699766667     998545776567643345434553234422344
  64798666779   97776434665445532244323332123321233
  448 8557889  965444334543223321233221221112211111
 9349 745898887532233223332112211122211111001100000
 824  626 +++++++++++++++++++++++++++++++0000000000
 616  616 +85310000111111000000000000000+0000000000
 508  507 + 7421111122111000000000000000+0000000000
 409  509 +  753222222211100000000000000+0000000000
 40   60  +  975433332221100000000000000+0000000000
 30   60  +   86544333221110000000000000+0000000000
 30   60  +   76544333221110000000000000+0000000000
 40   609 +  864333332221100000000000000+0000000000
 508  508 + 8532222222211000000000000000+0000000000
 606  617 +96310001222111000000000000000+0000000000
 815  626 +++++++++++++++++++++++++++++++0000100000
 934  735998888642344333443123321233211221001110011
  448 8557888  974455434554334432344322332112211121
  547 9656778   97676435675456542355433553223321233
  64799766667    9898545787568753456434664335532354
  757997776558       656897679964466545875457643466
89757887787546   9   8679 878  75678656996569854688
787678767996458988    78  878  86799757 9768  657
776678657  74467669   99  868  979  868  769  758
775578646  95456548   9   868   8   978  869  868
8745896359 95466436   89  968   9    79  869  868
9744897348 955785248 878  968  98    8  869  868
 8448 8337 8569 63368657  968  97    8  968  868
 9438 94369746  84356435  968  869   7  968  868
  438  4368636   54664249 857  757  969  957  858
  438  5368625   547841379746  746  858  957  858
  538  547 6249 9559 62268535  6359 747  857  858
  548 9559 8338 846  833685249 62489635  857  858
  548 945  94369636  9437851379623795249 747  858
  548 845   5368525   558 612785237852489647  858
  549 844   5479524   559 722685237852378646  857
```

Incident from left, direction of propagation

Figure 4(d): Lit-positive representation of normalized intensity for objects of varying aspect ratio. A.R. = 1/3

```
  111  111   11    111
  111  111  121    111
  11   11   111    111
  11   11   11    111
  11   11   11    111   11
  11   11   1     11   111+
  1    1    1    121   111
 11   11   11    121   11
 11   11   11    121  1211
111  121   11    11   1211
121  121  122    11  122211
121  121  122    11  132211
121  121  121   111  1332211
121  121  121   121  1233221
121  121  121   121  1233221
121  111  121   221  1233321
121  111  121   231  23333221
121  111  221   231  23343321
111  121  221   221  23444321
121  121  221   221 134444321
121  221  221   221 134444321
121  221  221   221 134444321
231  231  231   221  23444321
232  231  231   221  23444321
232  231  231   221  13444321
342  232  231   231  +3444321  +
232  231  231   221  23444321
232  231  231   221  23444321
231  231  221   221  23444321
121  221  221   221 134444321
121  221  221   221 134444321
111  121  221   221 133444321
111  121  221   221  23444321
121  111  221   221  23343321
```

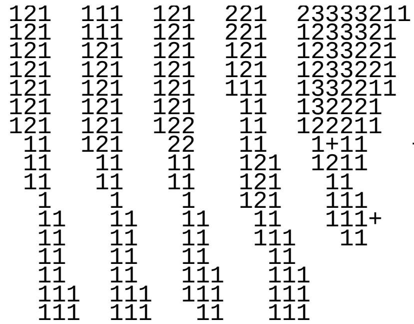

Figure 5(a) Lit-positive representation of normalized intensity for 2-D kidney-shaped object. A.R. =4, (b)

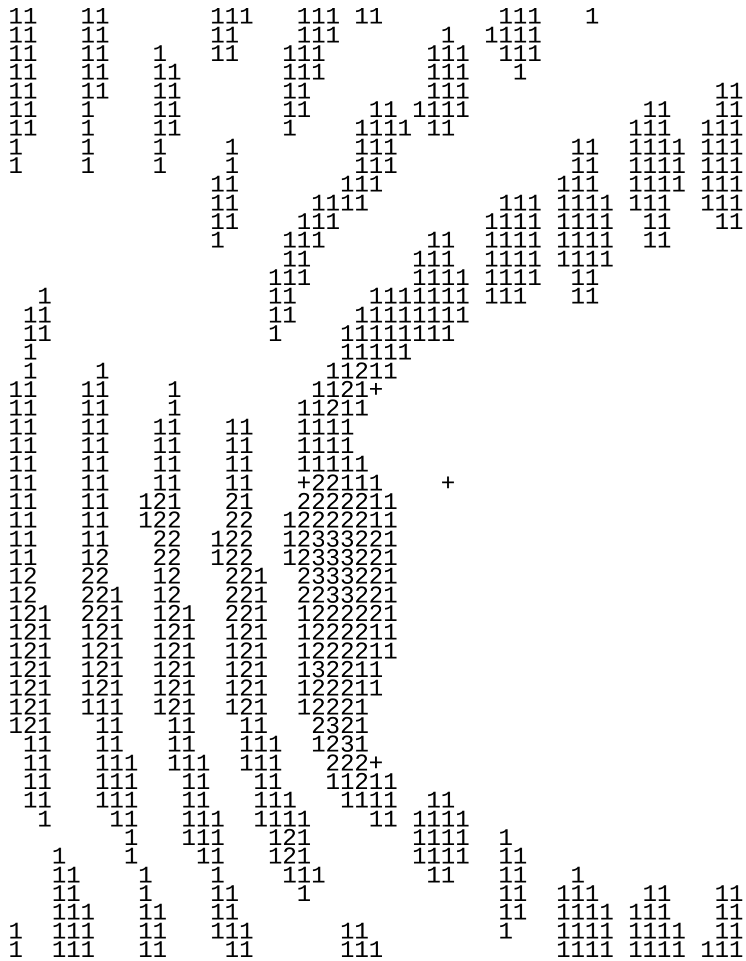

Figure 5(b): Lit-positive representation of normalized intensity for 2-D kidney-shaped object. A.R. =2.

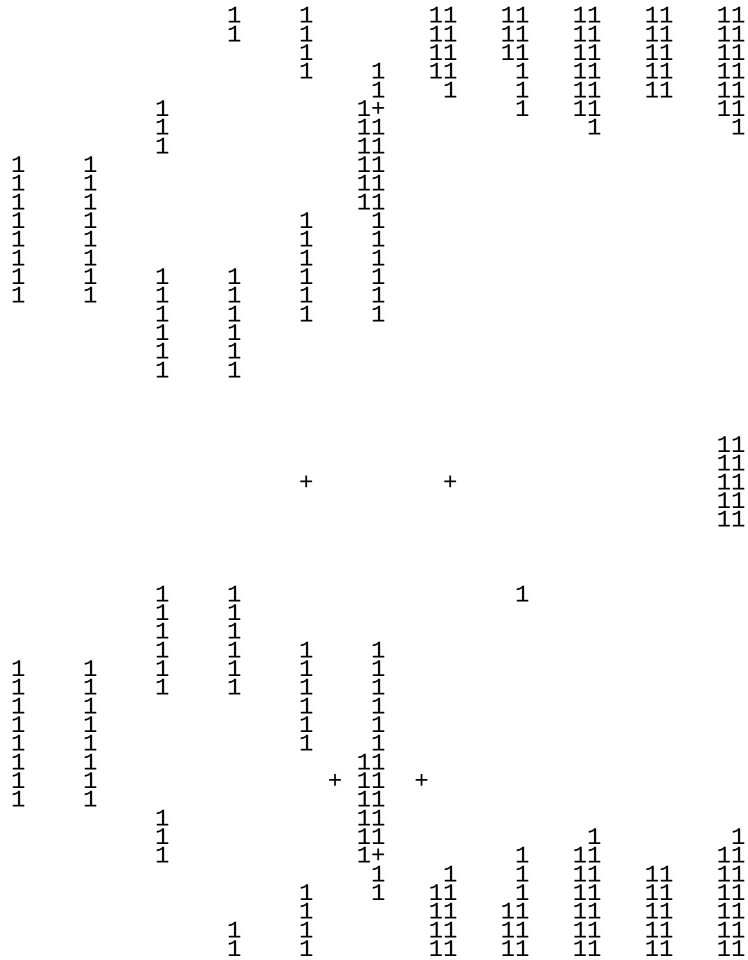

Incident from left, direction of propagation

Figure 6: Lit-positive representation of normalized intensity for kidney for A.R. = 4.

We observe that when an acoustically denser soft target is exposed to a time harmonic plane acoustic wave, there occurs inside the target high pressure band(s) whose magnitude is higher than the incident wave amplitude. These may induce compressional forces within a target and, if these exceed a certain target specific limit, the target might implode.

5.0 Acknowledgement

I acknowledge helpful discussions held with Dr I. Mbeledogu of the Department of Mathematics and Computer Science, University of Port Harcourt.

References

[1] Taflove A. (1995) *Computational Electrodynamics: The Finite Difference Time Domain Method*. Artech House: Boston, MA

[2] Ikata E. and Tay G. (1998) Il Nuovo Cimento 20D, N. 12, 1779.

[3] Yee K. S. (1966) IEEE Trans. Antennas Propagat., AP-13, 302.

[4] Lapidus L. and Pinder G. F. (1999) Numerical Solution of Partial Differential Equations in Science and Engineering. John Wiley: New York. p. 581

[5] Morgan M. A. (1989) in Finite Element and Finite Difference Methods in Electromagnetic Scattering – PIER vol. 2 M. A. Morgan (Ed.) Elsevier: Amsterdam p. 1

[6] Bayliss A. and Turkel E. (1980) Commun Pure Appl. Math., 33, 707.

[7] Mur G. (1981) IEEE Trans. Electromagnetic Compat., EMC-23, 377.

[8] Wells P. N. T. (1977) Biomedical Ultrasonics. Academic Press: New York